High-resolution photoacoustic vascular imaging in vivo using a large-aperture acoustic lens

Konstantin Maslov, Lihong V. Wang

Konstantin Maslov, Lihong V. Wang, "High-resolution photoacoustic vascular imaging in vivo using a large-aperture acoustic lens," Proc. SPIE 5697, Photons Plus Ultrasound: Imaging and Sensing 2005: The Sixth Conference on Biomedical Thermoacoustics, Optoacoustics, and Acousto-optics, (25 April 2005); doi: 10.1117/12.590558

SPIE.

Event: SPIE BiOS, 2005, San Jose, CA, United States

High-resolution photoacoustic vascular imaging in vivo using a large-aperture acoustic lens

Konstantin Maslov* and Lihong V. Wang
Optical Imaging Laboratory, Department of Biomedical Engineering
Texas A&M University, 3120 TAMU, College Station, Texas, USA 77843-3120

ABSTRACT

Reflection-mode photoacoustic microscopy with dark-field laser pulse illumination and high frequency ultrasonic detection is used to non-invasively image blood vessels in the skin *in vivo*. Dark-field illumination minimizes the interference caused by strong photoacoustic signals from superficial structures. A high numerical-aperture acoustic lens provides high lateral resolution, 45–120 micrometers in this system while a broadband ultrasonic detection system provides high axial resolution, estimated to be ~15–20 micrometers. The optical illumination and ultrasonic detection are in a coaxial confocal configuration for optimal image quality. The system is capable of imaging optical-absorption contrast at up to 3 mm depth in biological tissue.

Keywords: Medical and biological imaging, Photoacoustic imaging, Scanning microscopy.

1. INTRODUCTION

The ability to image the micro-vascular network in skin is invaluable in dermatology[1] and related cancer research.[2,3] One of the promising techniques for accomplishing this objective is photoacoustic microscopy. Current high-resolution optical imaging techniques, such as confocal microscopy and optical coherence tomography, can image only up to approximately one transport mean free path (~1–2 mm) into biological tissues, because these techniques depend on ballistic or quasi-ballistic photons. These techniques are sensitive to the backscattering that is related to tissue morphology, but they are insensitive to optical absorption which is related to important biochemical information. Photoacoustic imaging does not depend on ballistic or quasi-ballistic photons and can, therefore, penetrate deeper. Further, it provides high optical-absorption contrast while maintaining high ultrasonic resolution. Consequently, structures with high optical absorption coefficients, such as blood vessels, can be imaged clearly.

All imaging techniques have a common goal of maximum image clarity and resolution at the desired penetration depth within a reasonable time frame. High image resolution has been achieved previously with circular-scanning photoacoustic computed tomography.[4,5] Although a full 360-degree scan around an object provides high resolution and minimizes artifacts, it can be accomplished only on elevated objects, such as the brain or breast. Previously investigated planar reflection-mode techniques[6–8] are not limited by the shape of the sample, but they may suffer from strong photoacoustic waves emitted from optical absorbers near the surface—such as hair follicles or melanin, whose acoustic reverberations can potentially overshadow the much weaker photoacoustic signals from structures deep in the tissue.

Here, we report on a reflection-mode microscopic photoacoustic imaging technique that uses dark-field illumination, as in dark-field microscopy, to avoid the above problems. To achieve high image resolution and high sensitivity, we utilize a high frequency large numerical aperture (NA) spherically focused ultrasonic transducer that is coaxial and confocal with the optical illumination.

2. MATERIALS AND METHODS

2.1. Theoretical fundamentals

Due to the strong light scattering that occurs in biological tissue, beyond one optical transport mean free path into biological tissue, the photoacoustic image resolution is primarily determined by the ultrasonic detection parameters and the axial resolution is governed by a very familiar Abbe-Rayleigh lateral resolution criterion:

*maslov@tamu.edu, phone 1 979 845-4487, fax 1 979 845-4450

Photons Plus Ultrasound: Imaging and Sensing 2005, edited by Alexander A. Oraevsky, Lihong V. Wang, Proceedings of SPIE Vol. 5697 (SPIE, Bellingham, WA, 2005)
1605-7422/05/$15 · doi: 10.1117/12.590558

$$\xi = 0.66\frac{\lambda}{\sin(\theta)}, \tag{1}$$

where λ is the acoustic wavelength, and θ is the focusing transducer aperture angle. Obviously, the standard way to improve resolution is to increase the ultraonic frequencies used in photoacoustic microscopy. Simultaneously, this also increases the detectability of small $ka < 1$ optical absorbers because the amplitude of the high frequency components of he photoacoustic signal increases linearly with the ultrasonic frequincy[5]:

$$\tilde{p}(r,\omega) \sim -i\mu_a P_0 a^3 \frac{\omega\beta}{C_p}\frac{\exp(ikr)}{r}, \tag{2}$$

where P_0 is the optical energy fluence; β is the isobaric volume expansion coefficient; μ_a is the optical absorption coefficient, $k = \frac{\omega}{c}$; a is the radius of the light absorbing sphere; and C_p is the specific heat.

Higher ultrasonic frequencies also expand the range of applications of quantitative photoacoustic measurements. As a simple example, an optically absorbing slab irradiated by a very short laser pulse will produce a photoacoustic pressure wave whose amplitude can be directly derived from basic equations[5] as:

$$\tilde{p}(\omega) = -iP_0\frac{\omega\beta}{2C_p}\frac{1-\exp(-d(\mu_a+ik))}{1-ik/\mu_a}, \tag{3}$$

where d is the slab thickness. From (3) one can see that for an optically thick slab, $d\mu_a > 1$, the photoacoustic signal is independent of the optical absorption coefficient unless the ultrasonic frequency is high enough to satisfy the $k/\mu_a >> 1$ condition.

However, increasing the ultrasonic frequency too much can result in an undesirably small penetration depth because the ultrasonic attenuation in biological tissue — 0.7 to 3 dB/(cm MHz) for human skin,[9] for example — increases linearly with the frequency. Therefore, a large NA is essential for the desired resolution. The tradeoff in using a large NA ultrasonic lens is the relatively small depth of focus, which limits the size of the B-scan image and in effect slows down the imaging process. Depth of focus can be increased by replacing the single-element focused ultrasonic transducer with an ultrasonic lens coupled to a multi-element annular piezoelectric transducer array. By introducing time-of-flight-dependent time delays between signals from the different transducer elements, one can dynamically focus theultrasonic transducer to a different depth for a single laser pulse, thus extending the area of the cross-sectional (B-scan) image while retaining the high lateral resolution of a spherically focused transducer. However, implementation of this technology is out of the scope of this paper.

2.2. Experimental equipment

Figure 1 shows the experimental setup for our photoacoustic microscopic system. A Q-switched pulsed Nd:YAG laser (Brilliant B, BigSky), operating at 532 nm, delivers, after a thousand-fold attenuation, 300 μJ light pulses to a 0.60-mm diameter optical fiber. The laser pulse width is 6.5 ns, and the pulse repetition rate is 10 Hz. The fiber output is coaxially positioned on a three-dimensional precision mechanical scanner with a focused ultrasonic transducer (Panametrics). The transducer has a center frequency of 50 MHz and a nominal bandwidth of 70% and is attached to an in-house-constructed concave lens (aperture diameter D = 5.5 mm and free working distance L = 5.6 mm). This aperture provides an NA of 0.44, which is considered relatively large in ultrasonics. The laser light from the fiber is expanded by a conical lens and then focused through an optical condenser with an NA of 1.1. The optical focal region overlaps with the focal spot of the ultrasonic transducer, thus forming a confocal optical dark-field illumination and ultrasonic detection configuration.

Compared with alternative designs involving bright-field illumination, the above design provides the following advantages. Firstly, a large illumination area reduces the optical fluence on the sample surface to less than 1 mJ/cm^2, which is well within the safety standards.[10] Secondly, a large illumination area partially averages out the shadows of

superficial heterogeneity in the image. Thirdly, dark-field illumination reduces the otherwise strong interference of the extraneous photoacoustic signals from the superficial paraxial areas.

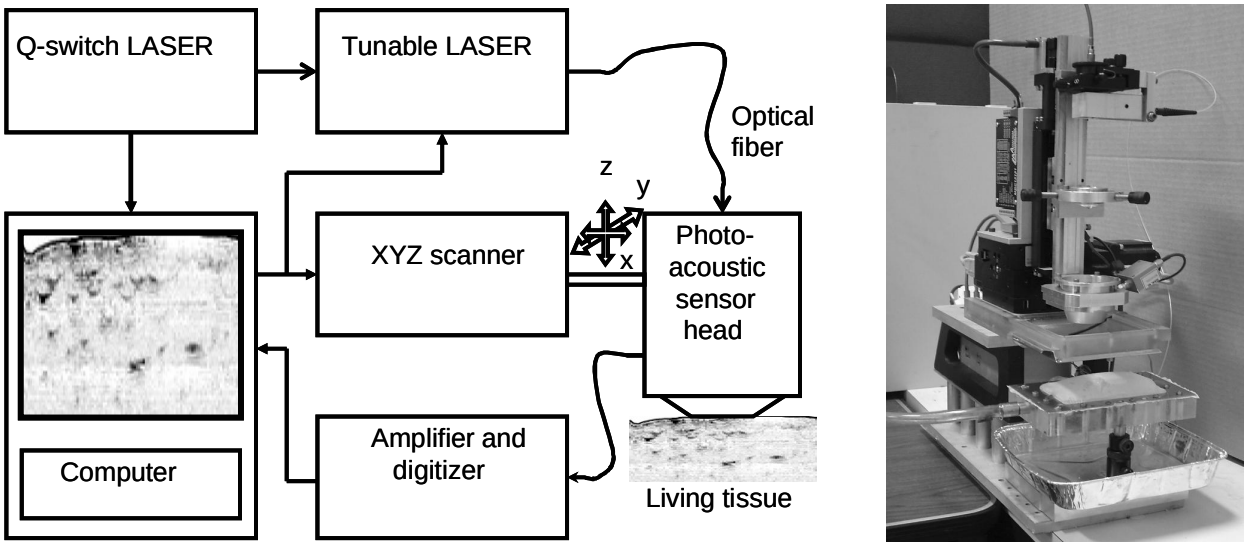

(a) (b)

Figure 1 Experimental setup for our photoacoustic microscopic system; (a) block diagram of the experimental setup; (b) picture of the imaging system.

Photoacoustic signals received by the ultrasonic transducer are amplified by a low-noise amplifier (ZFL-500LN, Mini-Circuits) and recorded by a digital oscilloscope. To avoid the influence of laser output power instability, part of the laser beam is diverted to a silicon photo-diode signal which is used to normalize the photoacoustic signal. The transducer is immersed in water in a plastic container with an opening at the bottom that is sealed with a thin disposable polyethylene membrane. The sample (animal) is placed outside the container below the membrane, and the ultrasonic coupling is further secured by coupling gel. Water temperature in the container is stabilized at 38°C.

2.3. Calibration

Figure 2(a) shows two photoacoustic images of a Mylar USAF-1951 test target. The lower part has been taken through a 4-mm thick layer of light diffusing tissue phantom made from 2% Intralipid solution (Clintec Nutrition Co., Dearfield, IL) in 1% agar gel. The estimated reduced scattering coefficient of the phantom[11], $\mu_s' \approx 1.5\,\mathrm{mm}^{-1}$, is greater than that of most biological tissues.[12] The thickness of the phantom translates into about six transport mean free paths. The numbers below the images in Fig. 2 indicate the spatial modulation frequency expressed in lines per millimeter. The solid curves show the relative ultrasonic pressure as a function of the horizontal displacement across the bars on the target. The modulation transfer function[13] was extracted from Fig. 2 and extrapolated to its cut-off spatial frequency, yielding an estimated lateral resolution of 45 μm. On the other hand, the axial resolution was estimated to be ~15 μm, based on the spread function of the photoacoustic signal from the top surface of an embedded object.

When a 1.2-mm thick freshly harvested skin from a sacrificed rat was placed between the acoustic lens and the USAF-1951 target (upper part of the image), the lateral resolution degraded to ~120 μm, which was likely due to increased ultrasonic attenuation. Ultrasonic attenuation in the skin decreased the signal-to-noise ratio (SNR) to ~30 dB from 80 dB in clear water and ~50 dB in the phantom samples. Increasing the SNR may potentially recover the resolution.

Figure 2(b) shows measured time-domain photoacoustic signals from two crossing 6 μm carbon fibers in water positioned on top of each other 10 μm apart. Traces 1 and 2 are experimentally measured signals from the first and second fibers separately, trace 3 is the sum of traces 1 and 2, and trace 4 is the experimentally measured signal taken at the lateral position where the fibers cross each other. One can see that trace 3 and 4 practically coincide. This proves the

intuitive notion that a photoacoustic imaging system has a linear response, that is, the photoacoustic signal from the superposition of two fibers is a linear superposition of the signals from each of them. Here, as is evident from figure 3(c), the photoacoustic signals from two cylindrical objects become separable when they are placed about 15μm apart, which defines the axial resolution of the current realization of the photoacoustic microscope.

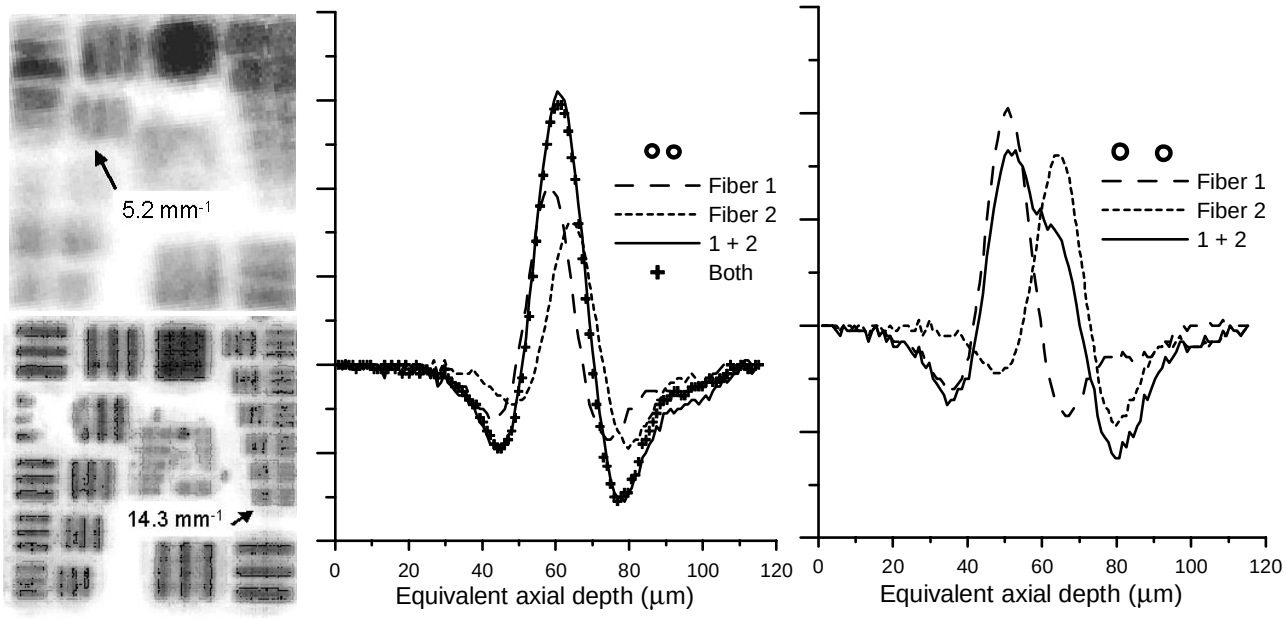

(a) (b) (c)

Figure 2 (a) Image lateral resolution test with a USAF-1951 bar chart embedded 4 mm deep in a tissue phantom. (b), (c) Image axial resolution test with two 6 μm diameter carbon fibers.

2.4. Animal protocol

Data were collected using Sprague Dawley rats (~180 g, Charles River Breeding Laboratories). Before imaging, the hair on the back of the rats was removed using commercial hair remover lotion. Imaging was performed under general anesthesia by intramuscular injection of ketamine hydrochloride (44 mg/kg), xylazine hydrochloride (2.5 mg/kg), acepromazine maleate (0.75 mg/kg), and atropine (0.025 mg/kg). During the procedure, the animal's normal body temperature was maintained by controlling the temperature of the immersion container, with additional heat provided as needed by an overhead surgical lamp. After several hours of experimentation, the rats recovered normally without noticeable health problems. Finally, the rats were sacrificed using pentobarbital (120 mg/kg, IP). The imaged skin was removed from the rats and photographed from the inner skin surface. All experimental animal procedures were carried out in compliance with the guidelines of the United States National Institutes of Health.[14] The laboratory animal protocol for this work was approved by the ULAC of Texas A&M University.

3. RESULTS AND DISCUSSION

Figure 3 shows photoacoustic images of the vascular distribution in the dorsal dermis (the upper lumbar area left of the vertebra) of a Sprague Dawley rat. Four *in vivo* consecutive photoacoustic B-scan images that were obtained 0.05 mm apart laterally are shown. Each image is a gray-scale plot of the envelope amplitudes of the received photoacoustic signals, where the vertical and horizontal axes represent the depth from the skin surface and the horizontal transducer position, respectively. The vertical axis was obtained by multiplying the acoustic time of arrival starting from the laser pulse with an assumed acoustic speed of 1500 m/s. The focal plane of the transducer was located at a depth of 1 mm. The animal was scanned horizontally with a step size of 0.05 mm for 200 steps: each of the B-scans took 20 s to complete. The solid line in the upper part of each B-scan delineates the skin surface. Some vessels, for example, the ones marked by 1 to 4 in Fig. 3, are nearly perpendicular to the imaging plane of the B-scans. One can see the splitting of the vessel marked 1,2 into two vessels 1 and 2 and the possible near-crossing of two blood vessels marked 3 and 4.

Note that the sizes of vessels 3 and 4 are ~0.05 mm (one pixel) in the image, indicating that the resolution in rat dermis is ~0.05-0.1 mm.

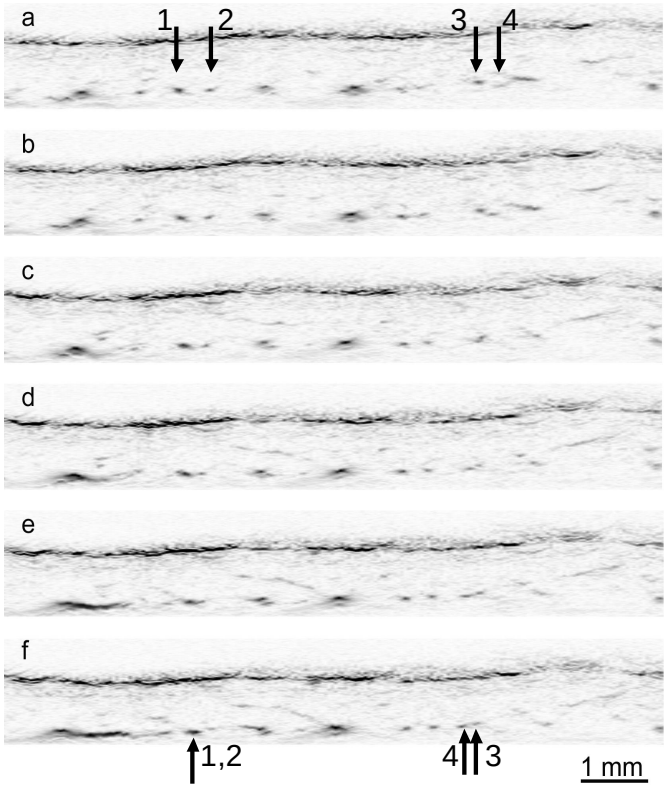

Figure 3. Six *in vivo* consecutive photoacoustic B-scans showing the vascular distribution in rat skin.

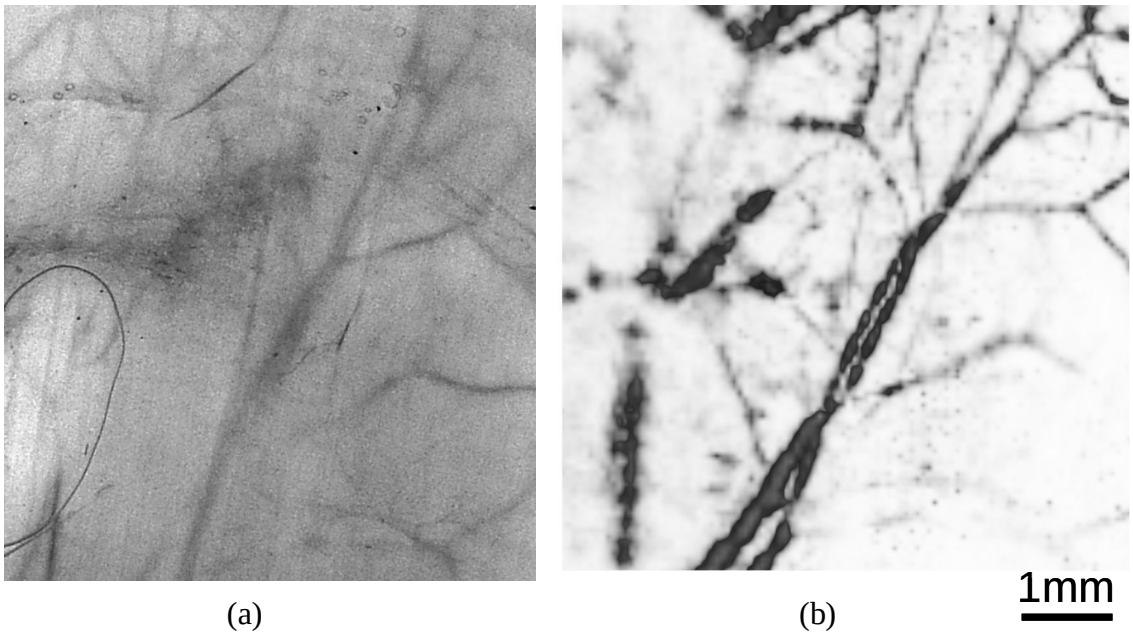

Figure 4. Vascular distribution in rat skin. Comparison of the (b) *in situ* photoacoustic projection image taken from the epidermal side and (a) photograph taken from the dermal side with transmission illumination.

The collection of B-scans similar to those shown in Fig. 3 forms a full three-dimensional image of the dermis and layers below. As shown previously[15], if a 50 MHz ultrasonic transducer is used to acquire the photoacoustic signals, the maximum useful penetration (imaging) depth in the tissue is about 3mm. The penetration depth is limited by the loss of resolution and signal magnitude due to frequency dependent ultrasonic absorption in soft biological tissue. At a 3 mm depth, the image resolution worsens to ~0.1-0.2 mm and the signal magnitude decreases by about 20 dB as compared to that at 1 mm depth. With the use of ultrasonic transducers with lower resonance frequencies, it is possible to improve the signal-to-noise ratio for deep imaging at the cost of reducing image resolution. For the 25 MHz transducer, the useful penetration depth was ~6 mm.

Figure 4(b) shows an *in situ* photoacoustic projection image similar to a C-scan or *en face* image (100 × 100 pixels, 0.1 mm step size). The image is a gray-scale plot of the maximum peak-to-peak amplitudes of the received photoacoustic signals within the 0.2–2 mm depth interval from the skin surface versus the two-dimensional transducer position on the skin surface. For comparison, Figure 4(a) shows a photograph of the inner surface of the harvested skin that was obtained using transmission illumination. Good agreement in vascular anatomy is observed between the photoacoustic image and the photograph. Based on the photograph shown in Fig. 4(a), the major vessels are ~100 μm in diameter, and the smaller vessels are ~30 μm in diameter.

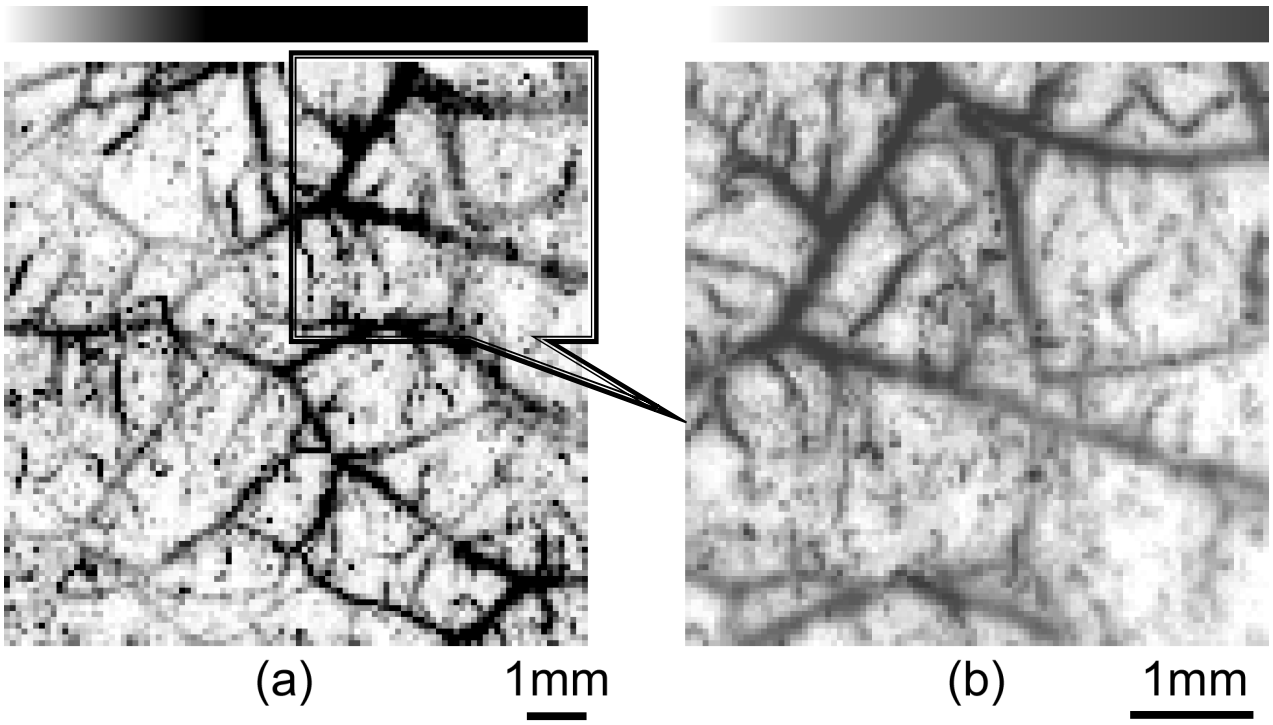

Figure 5. Vascular distribution in rat skin. *In vivo* non-invasive photoacoustic projection image.

Figure 5(a) shows an *in vivo* photoacoustic projection image of a similar area (100 × 100 pixel, 0.1 mm step size, 0.5–3 mm depth interval) taken *in vivo*. Figure 5(b) shows part of it taken with a smaller, 0.05 mm, step size. One can see an elaborate system of blood vessels with a density of up to a few counts per mm. The signal-to-background ratio for the larger vessels is ~40 dB.

Photoacoustic data obtained during mechanical scanning along the rat body forms a 3D array of data, (x,y axes and time of flight), and, in principle, full 3D reconstruction of the vascular anatomy is possible. Fig. 6 shows a 3D image of the superficial vascular network in the upper lumbar area of the Sprague Dawley rat. The image has been flipped so that the deepest structures are shown in front. This view shows blood vessels otherwise covered by an opaque triangular-shaped object that most plausibly is the end of the spinotrapezius muscle.

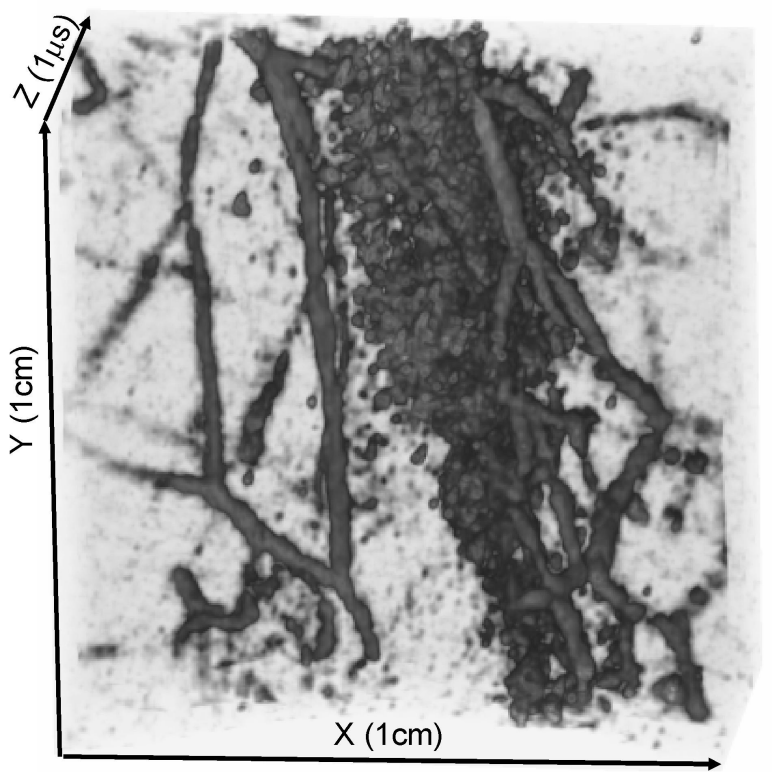

Figure 6. Three-dimensional reconstruction of vascular distribution below rat skin.

Although representation of a 3D bitmap image in the form of a collection of bounded objects is ambiguous, 3D pictures are easier to decipher, especially in view of possible medical applications of the technique. In the experiment, however, 3D reconstruction was complicated by the small depth of focus and motion of the rat body. Even though the rat skin was completely restrained outside the scanning area, it was not enough to completely immobilize body motion. For larger animals and humans, body motion should not present a significant problem.

4. SUMMARY

To summarize, a dark-field confocal microscopic photoacoustic imaging technique was developed to image biological tissues *in vivo*. The lateral resolution is as high as 45 μm in tissue phantoms. The maximum imaging depth is at least 3 mm. Further improvement of image resolution would be possible by increasing the ultrasonic frequency, at the cost of imaging depth. The photoacoustic images shown here were taken without signal averaging and, therefore, could be further improved by averaging, at the expense of data acquisition time. Our current imaging speed is limited by the pulse repetition rate of the laser that we used. Because lasers with pulse repetition rates of up to 100 KHz are now available, real-time photoacoustic imaging, which will reduce motion artifacts, is possible and extensive signal averaging is also realistic.

5. ACKNOWLEGEMENTS

This project was sponsored by the National Institutes of Health grants R01 EB000712 and R01 NS46214. Wang's email address is LWang@tamu.edu.

REFERENCES

1. H. Nakajima, T. Minabe, and N. Imanishi "Three-dimensional analysis and classification of arteries in the skin and subcutaneous adipofascial tissue by computer graphics imaging," *Plastic and Reconstructive Surgery*, **102**, 748-760, *(*1998).
2. P. Carmeliet and R. K. Jain "Angiogenesis in cancer and other diseases," *Nature* **407** (6801), 249-257, (2000).
3. S. J. Nelson and S. Cha "Imaging glioblastoma multiforme," *Cancer J.* **9,** 134–46, (2003).
4. X. Wang, Y. Pang, G. Ku, X. Xie, G. Stoica, and L. V. Wang, "Non-invasive laser-induced photoacoustic tomography for structural and functional imaging of the brain in vivo," *Nature Biotechnology* **21 (**7), 803-806 (2003).
5. M. Xu and L. V. Wang "Time-domain reconstruction for thermoacoustic tomography in a spherical geometry," *IEEE Trans. on Biomed. Eng.*, **50** (9), 1086-1099, (2002).
6. A. A. Oraevsky, V. A. Andreev, A. A. Karabutov, D. R. Fleming, Z. Gatalica, H. Singh, and R.O. Esenaliev "Laser opto-acoustic imaging of the breast: detection of cancer angiogenesis," *Proc. SPIE* **3597**, 352–63, (1999).
7. C. G. A. Hoelen, F. F. M. de Mul, R. Pongers, and A. Dekker "Three-dimensional photoacoustic imaging of blood vessels in tissue," *Opt. Lett.* **23**, 648–50, (1998).
8. R. G. M. Kolkman, E. Hondebrink, W. Steenbergen, and F. F. M. de Mul, "In vivo photoacoustic imaging of blood vessels using an extreme-narrow aperture sensor," *IEEE Journal on Selected Topics in Quantum Electronics* **9**, 343-346, (2003).
9. C. Guittet, F. Ossant, L. Vaillant, and M. Berson "*In vivo* high-frequency ultrasonic characterization of human dermis," *IEEE Trans. Biomed. Eng.* v.**46**, 740-746, (1999).
10. American National Standard for the Safe Use of Lasers, ANSI Standard Z136.D.H.
11. S. T. Flock, S. L. Jacques, B. C. Wilson, W. M. Star, M. J. C. van Gemert, "Optical Properties of Intralipid: A phantom medium for light propagation studies, " *Lasers in Surgery and Medicine* **12**, 510-519, (1992).
12. W. F. Cheong, S. A. Prahl, and A. J. Welch, "A review of the optical properties of biological tissues," IEEE J. Quantum Electronics 26, 2166-2185 (1990).
13. W. J. Smith, "Modern Optical Engineering," McGrew-Hill, New York, (1966), p. 318.
14. Guide for the Care and Use of Laboratory Animals, NIH Publication No. 86-23, revised. US Government Printing Office, Washington DC, (1985).
15. K. Maslov, G. Stoica and L.V. Wang, "In vivo dark-field reflection-mode photoacoustic microscopy," *Opt. Lett.* (2005), in press.